Article

Enhanced outcoupling in organic light emitting diodes via a high-index contrast scattering layer

Tae-Wook Koh, Joshua A Spechler, Kyung Min Lee, Craig B. Arnold, and Barry P. Rand

ACS Photonics, **Just Accepted Manuscript** • DOI: 10.1021/acsphotonics.5b00346 • Publication Date (Web): 13 Aug 2015

Enhanced outcoupling in organic light emitting diodes via a high-index contrast scattering layer

Tae-Wook Koh,[1†*] *Joshua A. Spechler,*[2,3†] *Kyung Min Lee,*[1] *Craig B. Arnold,*[1,2,3] *and Barry P. Rand*[1,3,4]

[1]Department of Electrical Engineering, [2]Department of Mechanical and Aerospace Engineering, [3]Princeton Institute for Science and Technology of Materials (PRISM), [4]Andlinger Center for Energy and the Environment, Princeton University, Princeton, New Jersey, 08544, USA

* Address correspondence to tkoh@princeton.edu, brand@princeton.edu

[†]Authors contributed equally to this work

KEYWORDS: organic light-emitting diodes (OLEDs), phase inversion, outcoupling efficiency, scattering layer

ABSTRACT: Despite high internal quantum efficiencies, planar organic light-emitting diodes (OLEDs) typically suffer from limited outcoupling efficiencies. To improve this outcoupling efficiency we develop a new thin (~2 μm) light scattering layer, which employs air voids (low-index scattering centers) embedded in a high-index polyimide matrix to effectively frustrate the substrate-trapped mode light, increasing the outcoupling efficiency. The porous polyimide

scattering layers are created through the simple and scalable fabrication technique of phase inversion. Optical properties of the scattering layers are characterized via microscopy, transmittance/haze measurements and ellipsometry, which demonstrate excellent scattering properties of these scattering layers. We integrate these films into a green OLED stack where they show a 65% enhancement in external quantum efficiency (EQE) and 77% enhancement in power efficiency. Furthermore we integrate these layers into a white OLED where we observe similar enhancements. Both the green and white OLEDs additionally demonstrate excellent color stability over wide viewing angles with the integration of this thin scattering layer.

Since the first observation of electroluminescence in organic solids[1] and the demonstration of a bilayer fluorescent organic light-emitting diode (OLED),[2] significant improvements have been realized in this thin film-based photonic device. The development of materials with improved transport properties,[3,4] chemical and thermal stabilities[5,6] and high luminescent quantum yields[7,8] have brought several important breakthroughs in device performance, while a deeper understanding of device physics and interfacial properties[9-11] have allowed for engineering devices to realize internal quantum efficiencies near the theoretical maximum of 100%.[12,13] While device electrical efficiency is approaching its limit, there is still significant room for improving optical efficiency, often referred to as outcoupling efficiency or light extraction efficiency. Outcoupling efficiency can be calculated with the aid of advanced modeling techniques[14-16] which show that only approximately 20-30% of emitted photons escape a non-cavity planar OLED fabricated on a conventional glass substrate.[17-19] Hence, in order to fully convert the input electrical power into optical power, it is essential to overcome this low outcoupling efficiency.

It should be noted that two factors are closely associated with typically low OLED outcoupling efficiency: the planarity of the device and refractive indices of the thin film stack. A planar organic/metal interface leads to evanescently coupled surface plasmonic losses,[20] while an index gradient starting from high-index organic layers to mid-index glass substrate to low-index ambient air leads to laterally travelling waveguided and substrate-trapped loss modes.[21] While the surface plasmonic loss mode can be reduced by spacing oscillating dipoles (i.e. emitters) away from the organic/metal interface or by introducing corrugation,[22] waveguided and substrate-trapped losses in bottom-emitting OLEDs require modifications to the optical structure in order to be recovered. One efficient way to deal with these two loss modes simultaneously is adopting a high-index substrate that can trade the waveguided mode for substrate-trapped mode while simultaneously applying an external extraction structure such as a pyramidal[23] or microlens array.[24] However fabricating these structures involve numerous processing steps and do not lend themselves toward low cost upscaling. An alternative approach is to use a composite scattering film,[25-28] where the index contrast between host medium (typically the substrate itself) and high-index nano/micro-particles induces scattering that redistributes the light propagating direction. Though this approach has been successful in improving outcoupling efficiency, it contradicts the desire for a high-index substrate and host medium: that is, as the index of the substrate/host medium gets higher, the smaller the index contrast between host medium and scattering particles becomes, leading to a less effective scattering-induced outcoupling efficiency enhancement.

Here, we demonstrate a simple yet effective method of fabricating flexible, polymeric scattering layers for OLEDs that require no costly patterning, etching, or molding processes, aspects that are desirable for mass-production of large-scale lighting panels. The chosen process

is that of phase inversion or, more specifically, immersion precipitation, which is widely used in the preparation of polymeric membranes for filter applications.[29] By using this technique, we have fabricated high-index polyimide films embedded with air voids. The large index contrast between the polyimide film and air void scattering sites results in an effective platform for ensuring effective scattering and outcoupling of waveguided light. The polyimide has a refractive index, n, greater than 1.7 and negligible absorption at wavelengths $\lambda > 460$ nm, making it a good candidate for the host medium of a scattering layer.

Results and Discussion

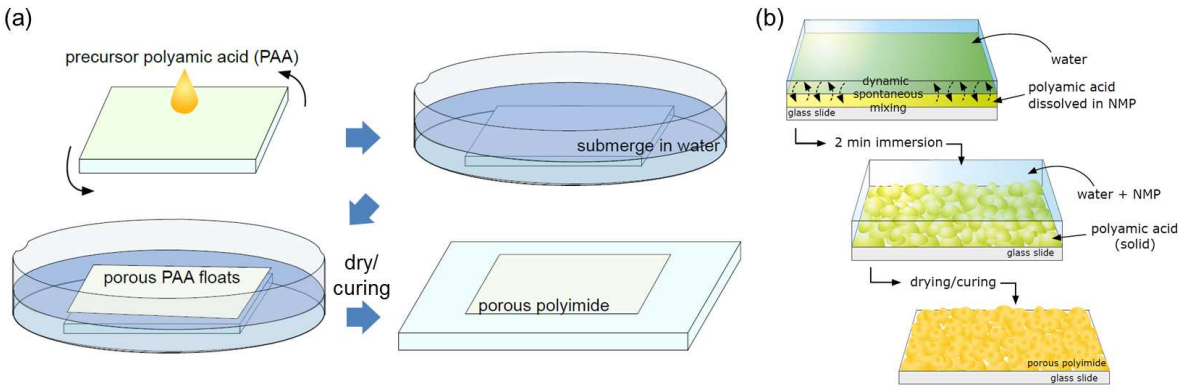

Figure 1. (a) Experimental schematic of the fabrication of a porous polyimide (p-PI) layer. (b) Stepwise illustration of the dynamic formation of porosity inside the p-PI layer.

Figure 1(a) shows the fabrication scheme of our porous polyimide (p-PI) films using the scalable phase inversion technique. We begin by spin coating a film of the polymer-solvent solution of interest. This film is then immersed in an anti-solvent that does not dissolve the polymer, but is miscible with the first solvent. The result of this process is a porous polymer structure. **Figure 1(b)** illustrates the dynamic formation of air voids within the precursor

polyamic acid films. In short, the physics of immersion precipitation relies on the interaction between a solution and an anti-solvent, a liquid that does not dissolve the solid material in the solution. Furthermore, the anti-solvent must be miscible with the solution solvent, and upon immersion of the solution in an anti-solvent bath the solid violently coagulates, and under the right choice of solution and anti-solvent this coagulated film can create a nano-porous structure.[30,31] Previous work has characterized the use of specific solvents and anti-solvents for polyimide precursor polyamic acid (PAA) solutions.[32,33] In this work, the PAA is dissolved in a polar aprotic solvent, n-methyl-2-pyrollidone (NMP). Water serves as an suitable and scalable anti-solvent for this system. The phase inversion PAA layer has a hazy appearance, which persists even after the thermal imidization step which converts the film into the p-PI film. While other studies need to maintain the contact between solvent and anti-solvent for as long as 24 h, our devices only require thin films of p-PI (~2 μm) which coagulate quickly and allow us to complete the process with only 2 minutes of immersion time.[34] The lamination of the PAA films to the glass substrates does not require any additional surface treatment or adhesive, and after the thermal imidization process adhesion between the p-PI film and the glass substrate is highly robust. Sonication of the substrates in hot (60 °C) baths of water, acetone or isopropanol had no effect on the p-PI film structure or the adhesion between the film and the glass.

The optical characterization of polyimide is summarized in **Figure 2(a-c)**. Refractive indices measured on a film via ellipsometry are shown in Fig. 2(a), The index, *n*, and extinction coefficient, *k*, are 1.74 and 0.002, respectively, at λ = 475 nm, the emission peak for the blue phosphorescent emitter FIrpic, and 1.73 and 0.0008 at λ = 510 nm, the emission peak for the green phosphorescent emitter $Ir(ppy)_3$. The refractive indices at these two representative wavelengths are indeed high enough to concentrate the optical power to the scattering layer,

while *k* values are small enough to justify the use of this polyimide as the host medium without significant parasitic absorption. This is also clear from the measured transmission (*T*) and absorption (*A*) of an 870-nm thick plain polyimide film (fabricated using the same spin coating conditions as the porous version) shown in Fig. 2(b), plotted together with the intrinsic photoluminescence spectra of FIrpic, $Ir(ppy)_3$ and $Ir(dmpq)_2(acac)$ blue, green, and red phosphorescent emitters, used in this work to construct a prototypical white OLED (WOLED).

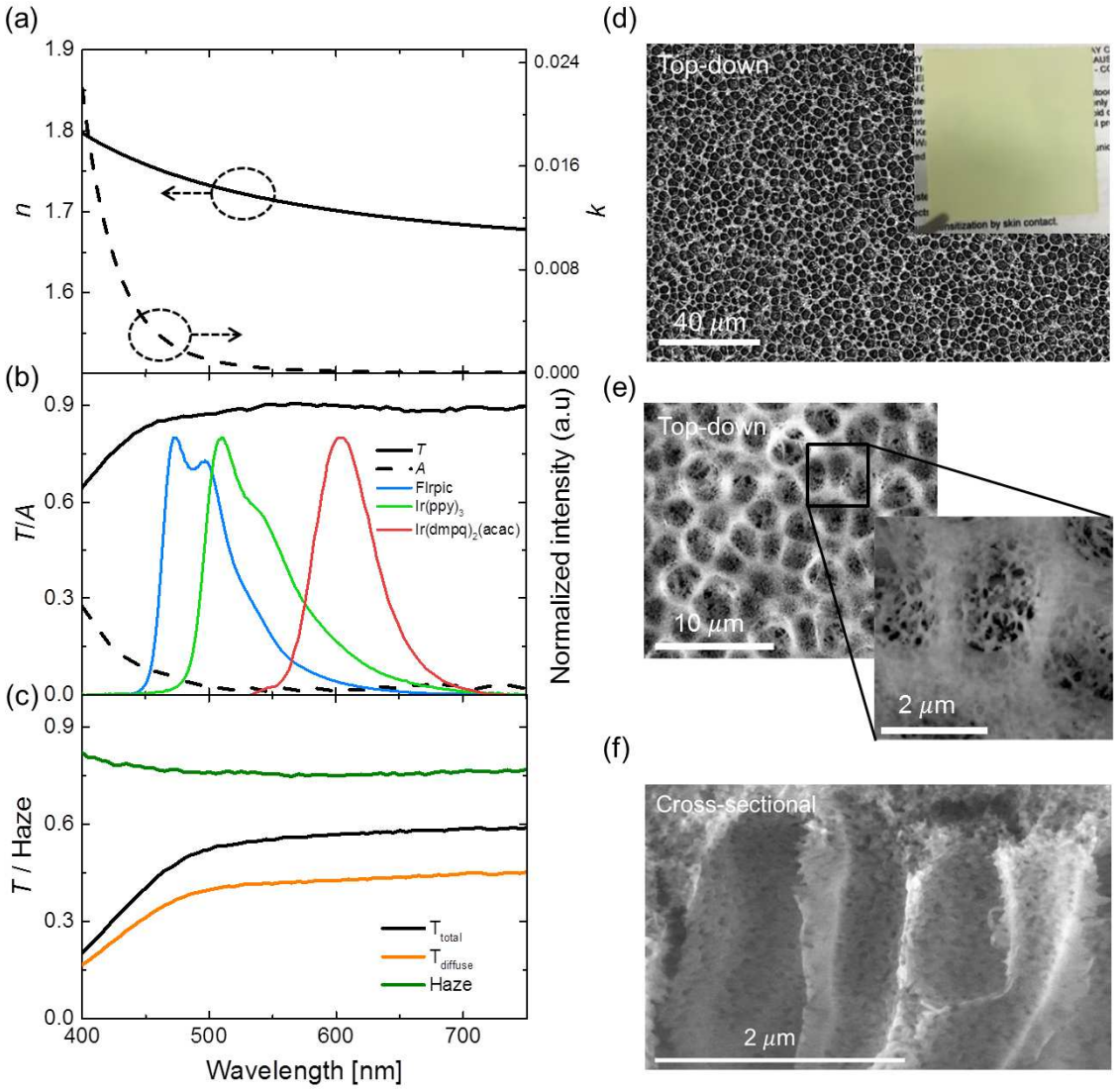

Figure 2. (a) Refractive index, *n*, and extinction coefficient, *k*, of the polyimide used in this work. (b) Transmission (*T*) and absorption (*A*) spectra of an 870-nm thick plain polyimide film and the intrinsic photoluminescence spectra of blue (FIrpic), green ($Ir(ppy)_3$), and red ($Ir(dmpq)_2(acac)$) phosphorescent dopants for the OLEDs employed in this work. (c) Measured total and diffuse transmission and calculated haze spectra for the p-PI scattering layer. (d) Top-down confocal microscope image (inset is a photograph of the p-PI layer on a glass substrate), (e) top-down SEM image, and (f) cross-sectional SEM image of the p-PI scattering layer.

We further characterize the p-PI layers via haze measurements and microscopy, as shown in Fig. 2(c-f) (inset image of Fig. 2(d) is a photograph of the p-PI film on glass). The confocal microscope image (Fig. 2(d)) reveals a highly porous framework characterized by voids of a few microns in extent. The structure is hierarchical in nature, consisting nanoscale voids clearly visible in the scanning electron microscope (SEM) images (Fig. 2(e, f)). The haze of the film is confirmed qualitatively in the inset photo to Fig. 2(d) and quantitatively in the haze data (Fig. 2(c)). Indeed, most of the transmission through the scattering film is diffuse, leading to an average haze of 77% in visible wavelength range as summarized. Throughout this work, we have utilized a 2 μm thick p-PI layer.

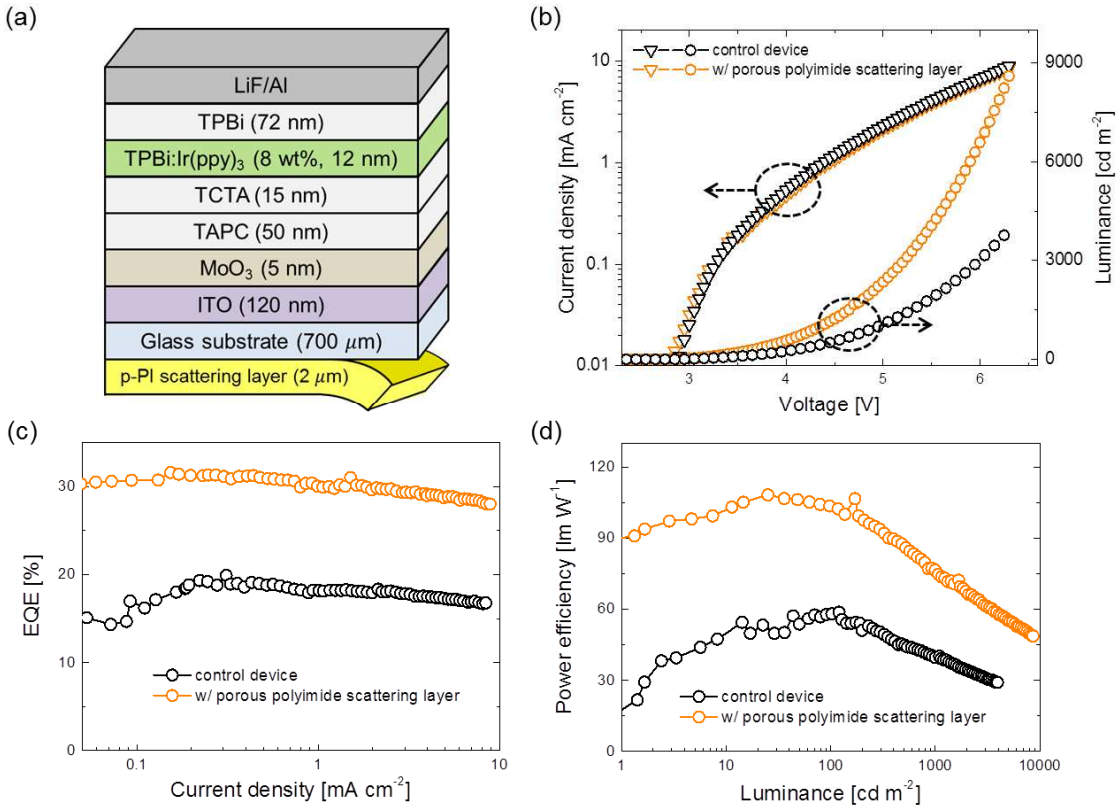

Figure 3. (a) Device structure of the green phosphorescent OLED with and without a p-PI scattering layer. (b) Current density (*J*) – luminance (*L*) – voltage (*V*) curves of the OLEDs. (c) External quantum efficiency (EQE) vs. *J*, and (d) Power efficiency vs. *L* for OLEDs with and without a p-PI scattering layer.

To verify their ability to enhance the optical outcoupling efficiency in OLEDs, we integrate the p-PI films on the backside of glass/indium tin oxide (ITO) substrates, as shown in the device schematic in **Figure 3(a)**. A 5 nm MoO_3 is used as a hole injection layer to inject holes into 50 nm-thick TAPC and 15 nm-thick TCTA hole transport layers. TPBi is used as both the phosphorescent host layer (12 nm) and electron transport layer (72 nm), and $Ir(ppy)_3$ is doped into TPBi at 8% by weight. The thicknesses of TAPC hole transport and TPBi electron transport layers have been designed to maximize the sum of the outcoupled and substrate-trapped modes while maintaining a high outcoupled mode portion in the green OLEDs, based on a power spectral density theory calculation[17] (**Figure S2**). Current density – forward luminance – voltage

(*J-L-V*) characteristics are given in **Figure 3(b)**, showing identical *J-V* but different *L-V* graphs for OLEDs with and without the p-PI layer as is expected since the modification is external. External quantum efficiency (EQE) and power efficiency (PE) are plotted versus *J* and *L* in **Figure 3(c)** and **3(d),** respectively, to give a comprehensive understanding of the outcoupling efficiency of the devices. The EQE of the control device at a current density of 1 mA cm^{-2} is 18.2%, and increased to 30.0%, an enhancement of 65%, after the p-PI scattering layer is applied to the substrate backside. The PE of the control device is measured to be 58.5 lm W^{-1} at a forward luminance of 100 cd m^{-2}, which increased to 103.6 lm W^{-1} with the aid of the p-PI layer. This enhancement ratio for power efficiency of 77% is higher than the case of EQE, simply because the same forward luminance is reached at a lower driving voltage and thus lower driving current for the p-PI layer-assisted device.

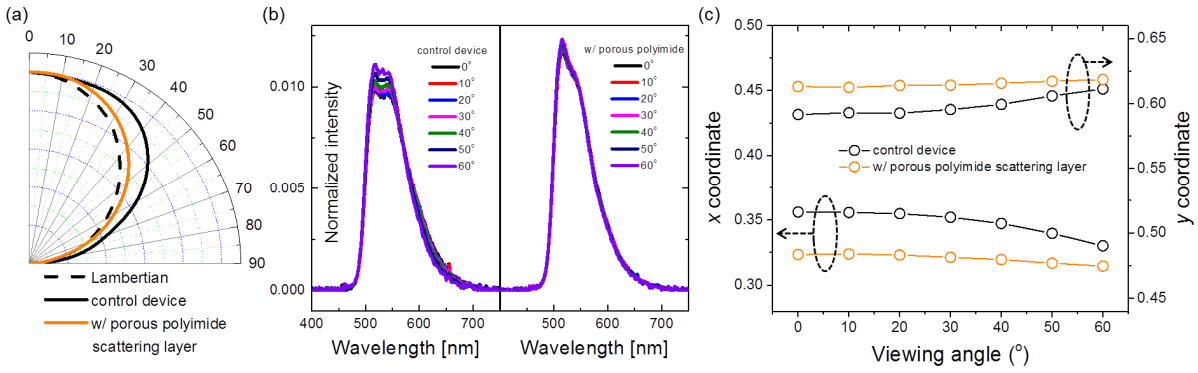

Figure 4. (a) Angular emission intensity profiles of green OLEDs normalized to the substrate normal emission. The dashed curve shows a Lambertian profile. (b) Electroluminescence spectra, and (c) CIE *xy* coordinates of OLEDs with and without the p-PI scattering layer, measured at viewing angles from 0° (substrate normal) to 60°.

Normalized angular emission intensity, normalized electroluminescence (EL) spectra and Commission International de l'Eclairage (CIE) 1931 chromaticity coordinates at different

viewing angles are provided in **Figure 4**. Even though the ITO electrode has a relatively high transmittance and low reflectance, there is nevertheless a weak microcavity effect,[35] as evidenced by the angular intensity profile being slightly wider than Lambertian. Additionally, there is a slight increase in the height of the dominant emission peak of $Ir(ppy)_3$ together with a narrowing of the longer wavelength tail as a function of viewing angle. After application of the p-PI scattering layer, the angular intensity adopts a nearly Lambertian profile. This is because the p-PI layer redistributes the light propagation randomly, leading to a considerably more uniform spectral distribution across the entire forward hemisphere as shown in Fig. 4(b). Furthermore, as shown in Fig. 4(c), the CIE 1931 *xy* coordinate (color diagram available in **Figure S3**) of the control device is (0.356, 0.592) at 0° (substrate normal) and (0.330, 0.611) at 60° with a Δxy of (0.026, 0.019), while the device with a p-PI scattering layer attached to it is (0.323, 0.613) at 0° and (0.315, 0.618) at 60° with a significantly smaller Δxy of (0.008, 0.005).

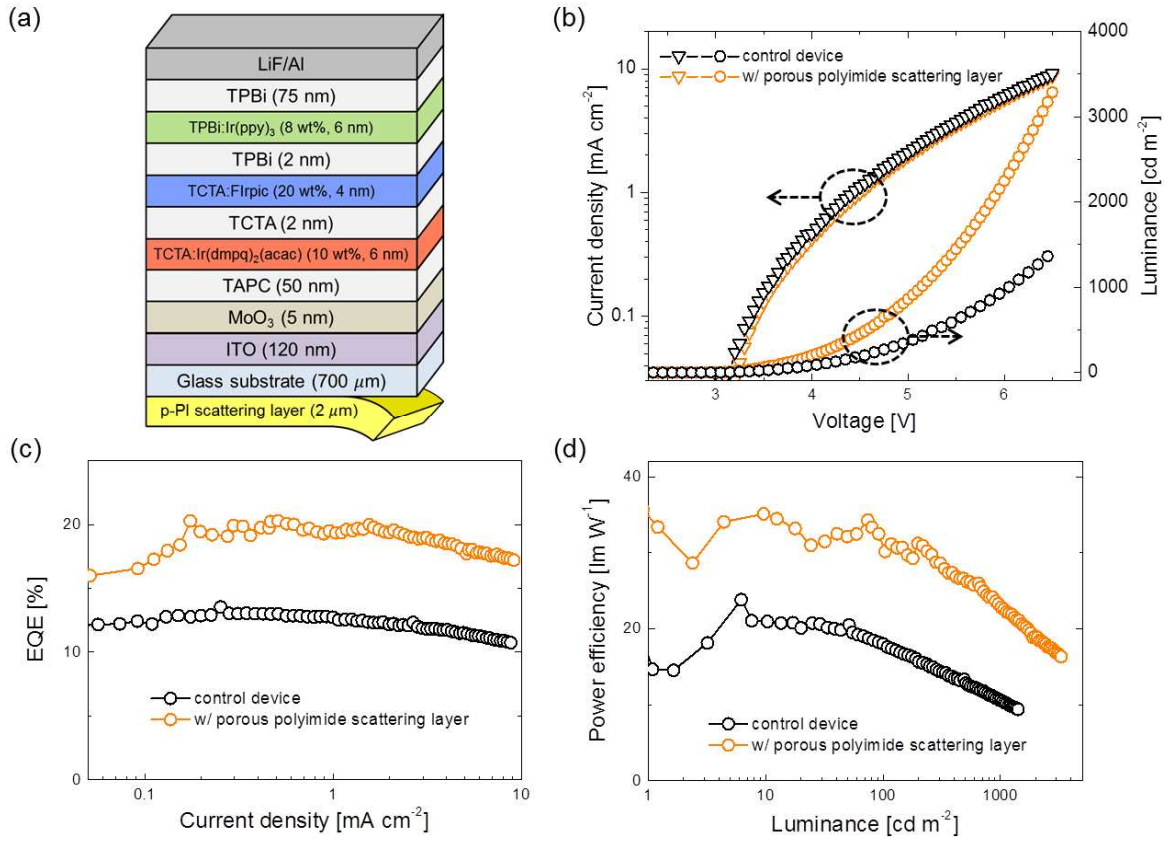

Figure 5. (a) Device structure of a WOLED with and without a p-PI layer on the back of the glass/ITO substrate. (b) Current density (J) – luminance (L) – voltage (V) characteristics of the WOLEDs. (c) External quantum efficiency (EQE) vs. J, and (d) Power efficiency vs. luminance curves for WOLEDs with and without a p-PI scattering layer.

Based on the enhancements observed for green OLEDs with the p-PI layer, we also demonstrate WOLEDs to prove the effectiveness of our approach for a broadband emission spectrum. The WOLED device structure, J-L-V graphs, EQE-J and PE-L graphs are shown in **Figure 5**. The phosphorescent dopants $Ir(dmpq)_2(acac)$, FIrpic and $Ir(ppy)_3$ are respectively used as red, blue and green emitters. In this structure, excitons are generated in TCTA and TPBi hosts within the vicinity of the TCTA/TPBi interface, to be utilized directly on FIrpic molecules or to be diffused away from the interface to generate red and green emission as has been described previously.[36] A 50 nm-thick TAPC and 75 nm-thick TPBi are used for hole transport and

electron transport layers, respectively. The glass/ITO control device has an EQE of 11.9% at a current density of 3 mA cm^{-2}, and the p-PI layer assisted device increased the EQE to 19.0% at the same current density, corresponding to a 60% enhancement of the optical outcoupling efficiency. This enhancement ratio is similar to the previous case of the green OLED, confirming that absorption loss within the p-PI layer is negligible while the scattering mechanism operates equally well across the broadband white spectrum. The PE of the control device at a forward luminance of 100 cd m^{-2} is 18.0 lm W^{-1}, whereas it increased to 32.1 lm W^{-1} for the p-PI assisted device, corresponding to a 78% enhancement.

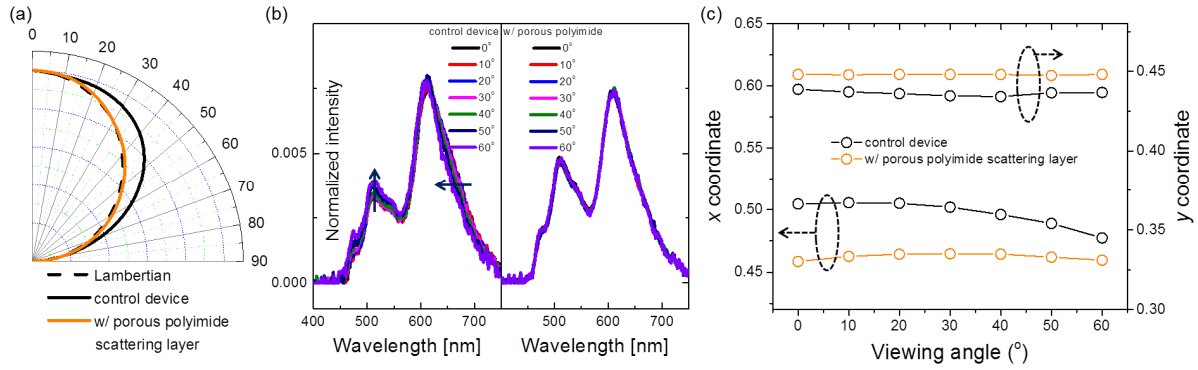

Figure 6. (a) Angular emission intensity profiles of WOLEDs normalized to substrate normal emission. The dashed curve shows a Lambertian emission profile. (b) Electroluminescence spectra, and (c) CIE *xy* coordinates of WOLEDs without and with the p-PI scattering layer, measured at viewing angles from 0° (substrate normal) to 60°.

The angular emission intensity profile, EL spectra and CIE 1931 coordinates of the WOLEDs are displayed in **Figure 6**. The angular intensity profile of the control WOLED, initially broader than Lambertian, is similarly narrowed due to the application of the p-PI layer, and the EL spectra at different viewing angles overlap identically as shown in Fig. 6(b). The color consistency across viewing angle improved considerably. The CIE *xy* coordinates of the control WOLED (color diagram available in **Figure S3**, photo of a working WOLED in **Figure S4**) are (0.505, 0.439) at 0° and (0.477, 0.437) at 60° with a Δ*xy* shift of (0.028, 0.002), while for

the WOLED with a p-PI layer they are (0.462, 0.448) at 0° and (0.461, 0.448) at 60°, with a notably small Δxy shift of (0.001, 0.000), ideal for lighting applications.

To understand the balance of photon density within the thin film OLED structure and be able to determine the potential gains from a scattering-based outcoupling approach, we have calculated the portions of each loss and outcoupled mode in the case of a green phosphorescent OLED with the same optical simulation code used for Fig. S2. This calculation provides relative portions of outcoupled, substrate-trapped, waveguided and surface plasmonic loss modes for a given device structure and power spectral dissipation density with respect to in-plane wavevector at wavelengths of interest. The power spectral dissipation density at a representative wavelength of λ = 510 nm (the emission peak of $Ir(ppy)_3$) is plotted in **Figure S5**, and these power dissipation densities are integrated over the designated in-plane wavevector ranges and summarized in **Table 1**, showing the relative portions of each mode in the device assuming a 100% internal quantum yield.

Table 1. Relative portions of outcoupled mode and energy loss modes in a green phosphorescent OLED, calculated using a power spectral dissipation density model.[17]

	Outcoupled	Absorption	Waveguided	Surface plasmonic	Substrate -trapped
Glass substrate	21.1%	4.6%	15.6%	27.2%	31.5%

From the calculated portions of loss modes we speculate that our p-PI scattering layer effectively recovered almost half (44%) of the substrate-trapped mode to enable a 65% enhancement in the outcoupled mode. Furthermore, through the introduction of a thicker, doped

transport layer to minimize surface plasmonic loss without compromising electrical efficiency,[16] and a high-index substrate to maximize the substrate-trapped mode, our high-index scattering layer with air void scattering centers can be further optimized for outcoupling efficiency.

In conclusion, we have employed the process of phase inversion as a straightforward, scalable and low-cost technique to fabricate flexible, polymeric scattering layers. Using polyimide as a high-index host medium and air voids as scattering centers, porous polyimide (p-PI) layers applied to green and broadband OLEDs show outcoupling efficiency enhancements of 65% and 60%, respectively. These enhancements are achievable owing to the large refractive index difference (>0.7) between the high-index polyimide host medium and low-index air voids, and also to the fact that the index of polyimide is greater than that of the glass substrate, beneficial for extracting substrate-trapped light into the scattering layer. In addition to the enhanced outcoupling efficiency, excellent color consistency between 0° and 60° viewing angles is also confirmed via a small Δxy shift of (0.001, 0.000) for the WOLED. An optical simulation based on power spectral density theory suggests that utilizing a substrate with a higher index compared to glass would lead to conversion of the waveguided mode into the substrate-trapped mode, which can be readily recovered by the proposed high-index scattering layer. Considering that high-index glass substrates are considerably more expensive than conventional substrates, WOLEDs on flexible, high-index plastic substrates with a scattering layer prepared by phase inversion can be an effective outcoupling enhancement strategy for future lighting applications.

Methods

Porous polyimide scattering layer fabrication and characterization: The precursor polyamic acid (PAA) (liquid PI2525, HD microsystems) dissolved in NMP (N-methyl-2-pyrollidone, Sigma Aldrich) was spun onto a glass microscope slide at 1000 rpm for 90 s. Then the slide was immersed in a water bath for at least 2 min. The porous, hazy phase inversion PAA film floated to the air/water bath interface. The film was then transferred onto the backside of an ITO coated substrate. The film was thoroughly dried under vacuum at 50 °C and then cured at 160 °C and 360 °C each for 20 min in a furnace, which thermally imidized the PAA creating a hazy, porous polyimide layer. An integrating sphere and calibrated Si photodiode (Labsphere) used together with a monochromator (TLS-300X, Newport) measured the total/diffuse transmission, absorption and haze. Confocal microscopy was performed with an Olympus LEXT scanning laser confocal microscope with a 50× N.A. = 0.95 objective under 405 nm laser illumination. SEM images were obtained with a FEI Quanta environmental SEM. Samples were prepared by freezing in liquid nitrogen and then cleaving to obtain an edge-on image. The low vacuum large field secondary electron detection mode was used to image the uncoated, non-conductive polyimide. The chamber pressure was set to 0.83 Torr and the electron beam was accelerated at 10 kV.

Device fabrication and analysis: Once the porous polyimide scattering layers were lifted from the bath on the backside of ITO substrates and cross-linked, they remained stable and intact against the physical and chemical cleaning processes. Substrates with patterned ITO electrodes in the front were cleaned using soapy water, DI water, acetone and isopropanol in sequence using an ultrasonicator for 20 min each, and then treated with O_2 plasma for 5 min. Then the

substrates were brought into a vacuum evaporation chamber (EvoVac, Angstrom Engineering, base pressure ≈ 5×10^{-7} Torr) for thermal evaporation of MoO_3 (Alfa Aesar), TAPC (4,4'-cyclohexylidenebis[N,N-bis(4-methylphenyl)benzenamine], Nichem) TCTA (4,4',4"-tri(9-carbazoyl)triphenylamine, Nichem), and TPBi (2,2',2"-(1,3,5-benzinetriyl)-tris(1-phenyl-1-H-benzimidazole), Nichem). $Ir(ppy)_3$ (tris[2-phenylpyridinato-C^2,N]iridium(III), Nichem) was co-evaporated with TPBi for the green emissive layer, and FIrpic (Bis[2-(4,6-difluorophenyl)pyridinato-C^2,N](picolinato)iridium(III), Nichem) or $Ir(dmpq)_2(acac)$ (Bis(2-(3,5-dimethylphenyl)quinoline-C^2,N')(acetylacetonato)iridium(III), Nichem) were co-evaporated with TCTA at desired doping ratios for blue or red emissive layers, respectively. LiF/Al cathode contact was used for both green and white OLEDs with 0.1 cm^2 device area. All organic materials were purified using a thermal gradient tube furnace (Lindberg/Blue M, Thermo Scientific) before use. Fabricated devices were measured using a homemade motorized goniometer setup consisting of a Keithley 2400 sourcemeter unit, a calibrated Si photodiode (FDS-100-CAL, Thorlabs), picoammeter (4140B, Agilent) and a calibrated fiber optic spectrophotometer (UVN-SR, StellarNet Inc.)

Acknowledgements

We acknowledge funding for this work from the DOE EERE SSL program under the award #DE-EE0006672. J.S. and C.B.A. acknowledge support from the Rutgers-Princeton NSF IGERT on Nanotechnology for Clean Energy. B.P.R. acknowledges support from a 3M Nontenured Faculty Award.

Supporting Information

The Supporting Information is available free of charge on the ACS Publications website at DOI: 10.1021/acsphotonics.XXXXXXX.

References

1. Helfrich, W.; Schneider, G.; Recombination Radiation in Anthracene Crystals. *Phys. Rev. Lett.* **1965**, 14, 229-231.

2. Tang, C. W.; VanSlyke, S. A.; Organic electroluminescent diodes. *Appl*. *Phys*. *Lett*. **1987**, 51, 913-915.

3. Murata, H.; Kafafi, Z. H.; Uchida, M.; Efficient organic light-emitting diodes with undoped active layers based on silole derivatives. *Appl*. *Phys*. *Lett*. **2002**, 80, 189-191.

4. Oh, H. –Y.; Lee, C.; Lee, S.; Efficient blue organic light-emitting diodes using newly-developed pyrene-based electron transport materials. *Org*. *Electron*. **2009**, 10, 163-169.

5. Tao, Y.; Wang, Q.; Yang, C.; Wang, Q.; Zhang, Z.; Zou, T.; Qin, J.; Ma, D.; A Simple Carbazole/Oxadiazole Hybrid Molecule: An Excellent Bipolar Host for Green and Red Phosphorescent OLEDs. *Angew*. *Chem*. *Int*. *Ed*. *Engl*. **2008**, 47, 8104-8107.

6. Steuber, F.; Staudigel, J.; Stössel, M.; Simmerer, J.; Winnacker, A.; Spreitzer, H.; Weissörtel, F.; Salbeck, J.; White Light Emission from Organic LEDs Utilizing Spiro Compounds with High-Temperature Stability. *Adv*. *Mater*. **2000**, 12, 130-133.

7. Baldo, M. A.; O'Brien, D. F.; You, Y.; Shoustikov, A.; Sibley, S.; Thompson, M. E.; Forrest, S. R.; Highly efficient phosphorescent emission from organic electroluminescent devices. *Nature* **1998**, 395, 151-154.

8. Ulbricht, C.; Beyer, B.; Friebe, C.; Winter, A.; Schubert, U. S.; Recent Developments in the Application of Phosphorescent Iridium(III) Complex Systems. *Adv*. *Mater*. **2009**, 21, 4418-4441.

9. Meyer, J.; Hamwi, S.; Kröger, M.; Kowalsky, W.; Riedl, T.; Kahn, A.; Transition Metal Oxides for Organic Electronics: Energetics, Device Physics and Applications. *Adv*. *Mater*. **2012**, 24, 5408-5427.

10. Ma, H.; Yip, H. –L.; Huang, F.; Jen, A. K. –Y.; Interface Engineering for Organic Electronics. *Adv*. *Funct*. *Mater*. **2010**, 20, 1371–1388.

11. Erickson, N. C.; Holmes, R. J.; Engineering Efficiency Roll-Off in Organic Light-Emitting Devices. *Adv*. *Funct*. *Mater*. **2014**, 24, 6074-6080.

12. Kawamura, Y.; Goushi, K.; Brooks, J.; Brown, J. J.; Sasabe, H.; Adachi, C.; 100% phosphorescence quantum efficiency of Ir(III) complexes in organic semiconductor films. *Appl*. *Phys*. *Lett*. **2005**, 86, 071104.

13. Yersin, H.; Highly Efficient OLEDs with Phosphorescent Materials. Wiley-VCH, Weinheim, Germany **2008**.

14. Benisty, H.; Stanley, R.; Mayer, M.; Method of source terms for dipole emission modification in modes of arbitrary planar structures. *J*. *Opt*. *Soc*. *Am*. *A*. **1998**, 15, 1192-1201.

15. Smith, L.H.; Wasey, J.A.E.; Samuel, I.D.W.; Barnes, W.L.; Light Out-Coupling Efficiencies of Organic Light-Emitting Diode Structures and the Effect of Photoluminescence Quantum Yield. *Adv*. *Funct*. *Mater*. **2005**, 15, 1839-1844.

16. Meerheim, R.; Furno, M.; Hofmann, S.; Lüssem, B.; Leo, K.; Quantification of energy loss mechanisms in organic light-emitting diodes. *Appl*. *Phys*. *Lett*. **2010**, 97, 253305.

17. Furno, M.; Meerheim, R.; Hofmann, S.; Lüssem, B.; Leo, K.; Efficiency and rate of spontaneous emission in organic electroluminescent devices. *Phys*. *Rev*. *B*. **2012**, 85, 115205.

18. Kim, S. –Y,; Jeong, W. –I.; Mayr, C.; Park, Y. –S.; Kim, K. –H.; Lee, J. –H.; Moon, C. –K.; Brütting, W.; Kim, J. –J.; Organic Light-Emitting Diodes with 30% External Quantum Efficiency Based on a Horizontally Oriented Emitter. *Adv*. *Funct*. *Mater*. **2013**, 23, 3896-3900.

19. Gather, M. C.; Reineke, S.; Recent advances in light outcoupling from white organic light-emitting diodes. *J*. *Photon*. *Energy*. **2015**, 5, 057607.

20. Hobson, P. A.; Wedge, S.; Wasey, J. A. E.; Sage, I.; Barnes, W. L.; Surface Plasmon Mediated Emission from Organic Light-Emitting Diodes. *Adv*. *Mater*. **2002**, 14, 1393-1396.

21. Sun, Y.; Forrest, S. R.; Enhanced light out-coupling of organic light-emitting devices using embedded low-index grids. *Nat*. *Photonics* **2008**, 2, 483-487.

22. Koo, W. H.; Youn, W.; Zhu. P.; Li, X. –H.; Tansu, N.; So, F.; Light Extraction of Organic Light Emitting Diodes by Defective Hexagonal-Close-Packed Array. *Adv*. *Funct*. *Mater*. **2012**, 22, 3454-3459.

23. Chen, M. –L.; Wei, A. –C.; Shieh, H. –P. D.; Increased Organic Light-Emitting Diode Panel Light Efficiency by Optimizing Structure and Improving Alignment of Pyramidal Array Light-Enhancing Layers. *Jpn*. *J*. *Appl*. *Phys*. **2007**, 46, 1521-1525.

24. Möller, S.; Forrest, S. R.; Improved light out-coupling in organic light emitting diodes employing ordered microlens arrays. *J*. *Appl*. *Phys*. **2002**, 91, 3324-3327.

25. Bathelt, R.; Buchhauser, D.; Gärditz, C.; Paetzold, R.; Wellmann, P.; Light extraction from OLEDs for lighting applications through light scattering. *Org*. *Electron*. **2007**, 8, 293-299.

26. Shiang, J. J.; Duggal, A. R.; Application of radiative transport theory to light extraction from organic light emitting diodes. *J*. *Appl*. *Phys*. **2004**, 95, 2880-2888.

27. Liu, R.; Ye, Z.; Park, J. –M.; Cai, M.; Chen, Y.; Ho, K. –M.; Shinar, R.; Shinar, J.; Microporous phase-separated films of polymer blends for enhanced outcoupling of light from OLEDs. *Opt*. *Express* **2011**, 19, A1272-A1280.

28. B. W. Lim, M. C. Suh, Simple fabrication of a three-dimensional porous polymer film as a diffuser for organic light emitting diodes. *Nanoscale*, **2014**, 6, 14446-14452.

29. Strey, R.; Microemulsion microstructure and interfacial curvature. *Colloid*. *Polym*. *Sci*. **1994**, 272, 1005-1019.

30. Reuvers, A. J.; van den Berg, J. W. A.; Smolders, C.A.; Formation of membranes by means of immersion precipitation : Part I. A model to describe mass transfer during immersion precipitation. *J*. *Membrane Sci*.**1987**, 34, 67-86.

31. Smolders, C. A.; Reuvers, A. J.; Boom, R. M.; Wienk, I. M.; Microstructures in phase-inversion membranes. Part 1. Formation of macrovoids. *J*. *Membrane Sci*. **1992**, 73, 259-275.

32. Kim, S.; Jang, K. –S.; Choi, H. –D.; Choi, S. –H.; Kwon, S. –J.; Kim, I. –D.; Lim, J. A.; Hong, J. –M.; Porous Polyimide Membranes Prepared by Wet Phase Inversion for Use in Low Dielectric Applications. *Int*. *J*. *Mol*. *Sci*. **2013**, 14, 8698-8707.

33. Wang, H.; Wang, T.; Yang, S.; Fan, L.; Preparation of thermal stable porous polyimide membranes by phase inversion process for lithium-ion battery. *Polymer* **2013**, 54, 6339-6348.

34. Kim, J. H.; Min, B. R.; Park, H. C.; Won, J.; Kang, Y. S.; Phase behavior and morphological studies of polyimide/PVP/solvent/water systems by phase inversion. *J*. *Appl*. *Polym*. *Sci*. **2001**, 81, 3481-3488.

35. Bulović, V.; Khalfin, V. B.; Gu, G.; Burrows, P. E.; Garbuzov, D. Z.; Forrest, S. R.; Weak microcavity effects in organic light-emitting devices. *Phys*. *Rev*. *B*. **1998**, 58, 3730-3740.

36. Reineke, S.; Lindner, F.; Schwartz, G.; Seidler, N.; Walzer, K.; Lüssem, B.; Leo, K.; White organic light-emitting diodes with fluorescent tube efficiency. *Nature* **2009**, 459, 234-238.

Table of Contents